Highly efficient abnormal reflection via underwater acoustic metagratings

Junmei Cao, Hongyu Ma, Shuhuan Xie, Jiayan Li, Yong Li,* and Qian Cheng†
Institute of Acoustics, Tongji University, Shanghai 200092, China

(Received 13 December 2023; revised 10 February 2024; accepted 15 February 2024; published 8 March 2024)

The manipulation of the various forms of behavior of acoustic propagation holds significant importance in the realm of underwater acoustic communication and detection. Recent advancements have highlighted the efficacy of metamaterials and metasurfaces in precisely shaping acoustic wave fronts. However, unlike their counterparts in airborne environments, where air-solid boundaries are conventionally treated as rigid, underwater metastructures face challenges due to fluid-structure coupling, inevitably leading to near-field distortions. These distortions considerably impede the efficacy of manipulating acoustic wave fronts, especially at large angles. Here, we introduce an efficient underwater metasurface employing a grating structure that utilizes an overarching optimization strategy. Distinct from previous studies, this strategy comprehensively addresses both nonlocal interaction among all subunits and fluid-structure interaction. The employed methodology convincingly demonstrates the achievement of highly efficient abnormal reflections at various angles. The simulation results showcase an exceptional modulation efficiency exceeding 99% for the designed metagratings, encompassing a wide reflection-angle range of 45–85°. Additionally, experimental validation corroborates the effectiveness of these underwater metagratings. This study might present an effective technique for advancing underwater acoustic devices, offering a valuable contribution to the field.

DOI: 10.1103/PhysRevApplied.21.034015

I. INTRODUCTION

The manipulation of wave fronts in the desired ways holds great significance in both physics and engineering. In recent years, the development of metasurfaces has opened up new possibilities for manipulating acoustic waves [1–30]. Conventional metasurfaces are gradient metasurfaces designed based on the generalized Snell's law by introducing local phase shifts for each unit [4–6,31]. However, the coupling among all the subunits of the gradient metasurfaces, which sometimes can play a positive role in the wave-field control, is neglected in the design methodology. Consequently, the overall response of the metasurface is affected, as is typically observed in reflection models, where the efficiency of the reflected waves gradually diminishes with increasing expected angles [32].

To overcome the above limitations, the concept of the acoustic metagrating has been proposed [33–36]. Acoustic metagratings are periodically arranged lattice structures that are designed based on diffraction principles. In addition, acoustic metagratings consider the coupling among subunits within the period, providing a nonlocal approach to manipulating the acoustic field. This nonlocal design offers the advantages of simplicity and efficiency compared to local-gradient designs. It has demonstrated excellent performance in the design of an efficient metasurface in air, achieving highly efficient anomalous reflection [15,33–35,37]. The effectiveness of this approach is verified in airborne metasurfaces, in which the air-structure boundary can be reasonably treated as an ideal rigid boundary due to the huge impedance mismatch, leading to a close match between analytical solutions and simulated or experimental results.

Recently, the nonlocal design approach has also been extended into underwater acoustics [38,39]. It is noteworthy that, despite significant breakthroughs in acoustics made by metasurfaces, theoretical and experimental studies of underwater acoustic metasurfaces are still in the initial stages of development. Compared to airborne acoustic metasurfaces, the application of underwater metasurfaces faces substantial difficulties. This is primarily due to the relatively small acoustic impedance difference between solid structures and water, which prohibits the treatment of structures in water as ideal rigid bodies. For instance, an acoustic metagrating composed of iron cylinders has been proposed to achieve directional control of underwater acoustic waves. It has been found that the elastic properties of the cylinders play a significant role in influencing their ability to manipulate acoustic field. Cylinders with identical geometric parameters but different materials exhibit distinct capabilities in reshaping

*yongli@tongji.edu.cn
†q.cheng@tongji.edu.cn

acoustic wave fronts [40]. Thus it can be seen that the interaction between metasurfaces and underwater acoustic waves is more complex than for their counterparts in air. The increased complexity makes it challenging to directly apply existing metasurface design methods to underwater acoustics, inevitably leading to performance degradation, failure, and reduced efficiency in wave-front manipulation. For instance, the effective deflection of acoustic waves toward large angles becomes particularly difficult under water.

In this study, we propose a distinct approach for designing underwater metagratings, drawing inspiration from airborne acoustics and carrying out modifications to better suit the underwater situation. Considering the interactions between water and solids, we have employed a combination of finite-element simulation and a genetic algorithm to design and optimize the structural parameters, further improving the performance of the metagratings. Compared with previous research, we have adopted an overarching design strategy, integrating considerations of the coupling of units and fluid-solid interactions. By rational design of the underwater metagratings, we have achieved anomalous reflections at the desired angles of 45°, 60°, and 85°. Our approach has overcome challenges in traditional design methods for attaining large-angle anomalous reflection, with an efficiency exceeding 99% in the simulations. Furthermore, to ensure the performance of the designed metagratings, we have conducted experimental validations. The simulation and experimental results confirm the effectiveness of the underwater metagratings, demonstrating their potential for applications in underwater acoustics and biomedical ultrasound diagnosis. Additionally, the optimization design strategy also showcases substantial promise and provides valuable insights for future underwater acoustic research and device advancement.

II. DESIGN STRATEGY

We have utilized the metagrating depicted in Fig. 1 to achieve underwater anomalous reflection. In Fig. 1(a), the periodically arranged grid structure is displayed for redirecting normally incident waves in the desired direction. Figure 1(b) represents a unit cell of the metagrating, with a periodic length of a. It comprises two rectangular grooves (subunits) with depths l_1 and l_2, widths t_1 and t_2, and spacing d. Designing the metagrating based on diffraction theory has established that, for an incident angle θ_i, the acoustic field conforms to the equation [31,34]

$$\sin\theta_r - \sin\theta_i = n\frac{2\pi}{ka}, \tag{1}$$

where $n = 0, \pm 1, \pm 2, \ldots, \pm\infty$ represents the diffraction order and k is the wave number of the incident wave, with θ_r denoting the reflection angle. Previous studies have shown that under the assumption of completely rigid structural boundaries, the parameters l_m, t_m, and d satisfy [34,35]

$$p_s(x,y) = A_0^+ e^{-jk_0 x\sin\theta_i} e^{jk_0\, y\cos\theta_i} + \sum_n A_n^- e^{-j(k_0\sin\theta_i + G_n)x} e^{-jk_{yG_n}y}, \tag{2}$$

$$p_g^m = \sum_n H_{nm}\cos[\alpha_{nm}(x - x_m)] \times \left(e^{j\beta_{nm}y} + e^{-j\beta_{nm}(y+2l_m)}\right), \tag{3}$$

where p_s is the acoustic pressure in the free field, p_g^m is the acoustic pressure inside the mth groove (where m is the number of grooves), $G_n = n2\pi/a$ is the wave number of the structure, A_0^+ is the amplitude of the incident wave, A_n^- is the amplitude of the nth-order refractive wave, x_m is the position of the mth groove in the x direction, k_0 is the wave number of the incident waves, and $k_{yG_n} = \sqrt{k_0^2 - (k_0\sin\theta_i + G_n)^2}$ is the wave number of the free field in the y direction. H_{nm} denotes the amplitude of the nth-order component of the waveguide mode and $\alpha_{nm} = n\pi/t_m$ and $\beta_{nm} = \sqrt{k_0^2 - \alpha_{nm}^2}$ are the wave numbers in the x and y directions of the groove.

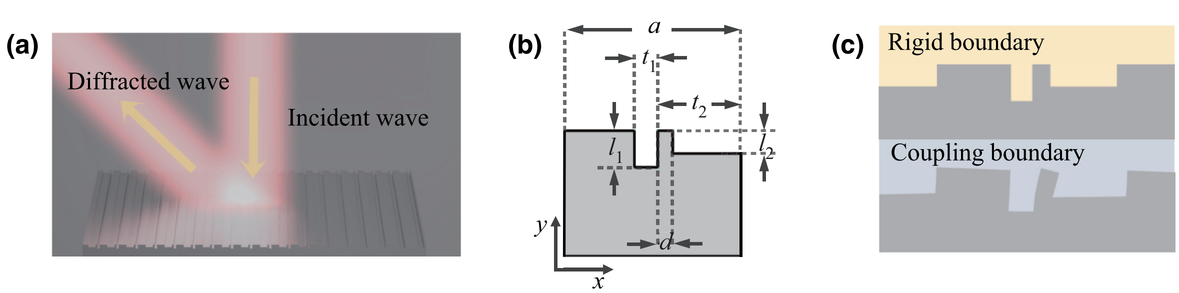

FIG. 1. The functional schematic of the proposed underwater metagrating. (a) The schematic diagram of the abnormal reflection. (b) The structural design parameters of the groove acoustic metagrating. (c) Schematic representations of the acoustic metagrating under hard-boundary and coupling-boundary conditions. While the metagrating is considered rigid under the hard-boundary condition, the interaction between water and the solid structure causes deformation of the structure, thereby not fulfilling the criterion for complete rigidity. By regulating the interaction between the water and the structure, wave-front control can be effectively promoted.

Therefore, by adjusting the period a, the acoustic wave front can be manipulated, redistributing the incident wave front to the desired angle, while effectively suppressing the reflections from other orders. The utilization of diffraction theory incorporates the interactions within the units, avoiding the design of unit discretization. This significantly enhances the efficiency of the acoustic field manipulation. Due to the inherent differences between the water and air environments, it is difficult to achieve perfect rigid boundary conditions in water. The structural vibrations induced by the acoustic field can exert an influence on the acoustic field itself. When acoustic waves interact with a structure, vibrations are induced in the structure, resulting in alterations to the surrounding acoustic field. These vibrations introduce additional acoustic waves, modifying the propagation direction and amplitude of existing acoustic waves. As shown in Fig. 1(c), the stress and load within the structure excite acoustic waves in the environment, causing the reflected waveform to be disturbed, which is different from the reflection of rigid boundaries. In this paper, the fluid-structure interaction (FSI) effect in water is employed, i.e., considering the acoustic-structural interaction and the interaction between different structural components. The metagratings are optimized in the overarching design to achieve efficient wave-front regulation.

The metagratings have been designed and validated using MATLAB and COMSOL MULTIPHYSICS. The simulation considers the background medium as water with a density of 1000 kg/m^3 and an acoustic velocity of 1414 m/s. The structure is made of steel, with a density of 7850 kg/m^3, a Young's modulus of 205 GPa, and a Poisson ratio of 0.28. For other materials, similar methods can be employed to achieve high-efficiency wave-front manipulation. The interaction between the water and structure is considered by incorporating the acoustic-structural coupling module within the multiphysics framework. This module establishes a connection between the acoustic pressure variations in the fluid domain and the structural deformations in the solid domain. The acoustic pressure in the fluid can exert fluid loading on the solid (structure), while the structural acceleration is applied as the normal acceleration across the fluid-structure interface to the water. Consequently, the coupling involves considering both the loads on the structure due to acoustic pressure and the structural acceleration imposed on the fluid domain [41], which can be described by the boundary conditions

$$\mathbf{F}_{\mathrm{A}} = p_{\mathrm{t}}\mathbf{n} \tag{4}$$

$$-\mathbf{n}\cdot\left(-\frac{1}{\rho_{\mathrm{c}}}\nabla p_{\mathrm{t}}\right) = a_n, \tag{5}$$

where $\mathbf{F}_A$ is the load borne by the structure, p_t is the total acoustic pressure, and n is the surface normal. The normal acceleration $a_n = (\mathbf{n}\cdot\mathbf{u})\omega^2$, where $\mathbf{u}$ is the displacement vector of solids and ω is the angular frequency of acoustic waves.

To ensure that the designed metagratings can efficiently operate over a wide range of angles, including extreme angles, the desired directions for anomalous reflection are set as 45°, 60°, and 85°. Due to the complexity of underwater acoustic environments, obtaining an analytical solution through forward design is challenging. Therefore, the reverse-design approach has been adopted in our research approach. First, we employ the air-based approach combined with diffraction theory and the genetic algorithm (GA) to determine the structural parameters of the metagratings, which we refer to as air-based metagratings. Based on the aforementioned theory, we can search for parameters l_1, l_2, t_1, t_2, and d at different expected angles. The objective function is defined as $f = \mathrm{abs}\left(1-\left|A_{-1}^{-}/A_0^{+}\right|^2\right)\rightarrow 0$, in order to eliminate unwanted diffraction order and search for the desired structural parameters. Subsequently, the structural parameters obtained from the air-based metagratings are integrated into the multiphysics coupling model that considers the fluid-structure interaction. These parameters serve as the initial values for optimizing underwater metagratings. Finally, the performance of the metagratings is optimized using finite-element simulation. The objective function for the optimization process is the reflection coefficient, which is aimed at maximizing the reflection efficiency of the underwater metagratings. In this study, the metagrating thickness has been fixed at 2.8 mm and the transmission has been neglected due to the dominant reflection of energy rather than transmission through the metagratings.

III. SIMULATION RESULTS

Figure 2 showcases the field maps of the reflected wave fronts after the normally incident acoustic waves (500 kHz) are modulated by the metagratings, propagating in the desired direction. The modulation results for 45°, 60°, and 85° reflections are displayed in Figs. 2(a)–2(c), respectively. In the modeling area, the top and bottom boundaries are set as perfectly matched layers (PMLs), which are absorbing layers designed to reduce reflections, and the left and right sides of the modeling area are set as periodic boundaries.

The three panels in each of Figs. 2(a)–2(c), from left to right, demonstrate the following conditions. Panel I shows the air-based metagrating in an ideal environment where the structure surface acts as a hard boundary. This represents the behavior of the metagrating when there is no interaction between air and solid. Panel II represents the air-based metagrating in water. Here, the metagrating is placed in a water environment, and the interaction between the air-based structure and water leads to changes in the reflection response of the metagrating. Panel III showcases the overall optimized underwater metagrating

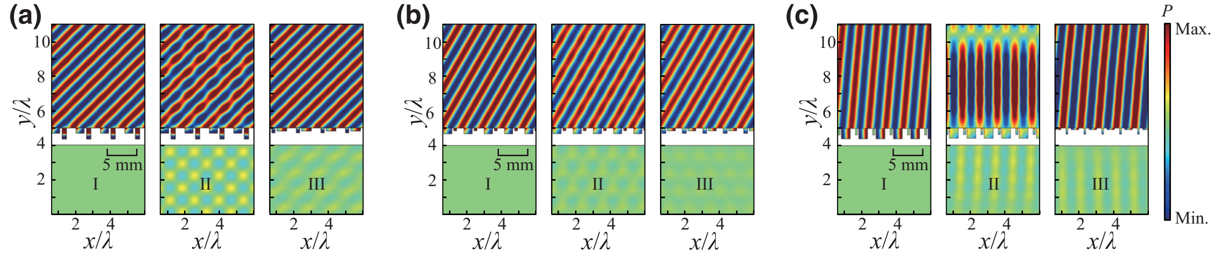

FIG. 2. The acoustic pressure fields of the anomalously reflected waves under normal incidence. The expected angle for anomalous reflection in the three sets are (a) 45°, (b) 60°, and (c) 85°, respectively. Panels I and II illustrate the reflection pressure fields of the structure designed without considering fluid-structure interaction under ideal conditions (the structure surface is a hard boundary) and in water (where the interaction between water and solid structures gives rise to unexpected orders of reflection). Panel III presents the reflection acoustic field in water of the underwater metagrating. The metagrating has been designed while considering fluid-structure interaction.

in water, where the desired reshaping performance of the metasurface has been achieved.

By comparing panel I with panel II, it can be observed that the fluid-structure interaction induces noticeable unexpected reflected waves in the anomalous-reflection acoustic field of the air-based metagratings. In panels II and III, the reflection efficiency of the designed underwater metagratings is evaluated in relation to that of the air-based metagratings. It is noteworthy that the designed underwater metagratings exhibit consistent and stable efficiency across a wide range of angles spanning from 45° to 85°. Furthermore, the underwater metagratings effectively suppress the occurrence of diffractive waves from unexpected orders.

The quantitative results of the reflection efficiencies for the 0th, −1st, and 1st orders of the metagratings are shown in Fig. 3. Figures 3(a)–3(c) display the reflection efficiencies for three observed angles, 45°, 60°, and 85°. To accommodate the significant differences in the data, a segmented y axis is employed. The range of 0–2 mainly represents the efficiency of unexpected reflections, while the range of 2–100 represents the efficiency of expected reflections. Notably, in Fig. 3(c), at the expected angle of 85°, the efficiency of the unexpected reflection orders has already reached 48% (yellow bar). This suggests that air-based metagratings exhibit a substantial occurrence of reflections that deviate from the desired direction. The same conclusion can also be demonstrated in Fig. 2(c), as the superposition of reflected waves from other directions leads to a noticeably different acoustic field in panel II compared to the other acoustic fields.

As the excepted angle increases, the air-based metagratings maintain efficient anomalous reflection in the hard-boundary-reflection model. However, in the underwater acoustic environment, the efficiency of the metagrating designed without considering fluid-structure interaction

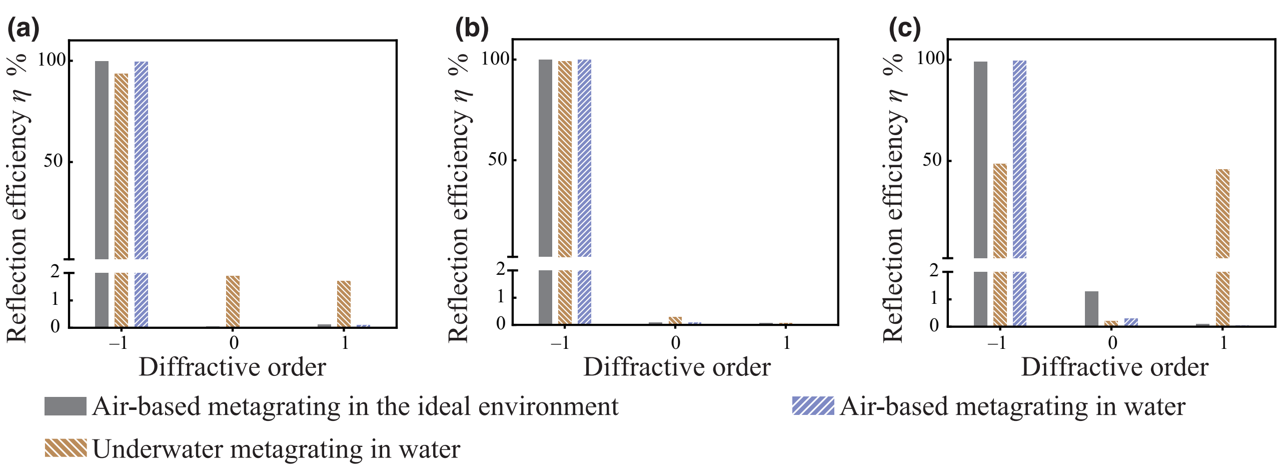

FIG. 3. The anomalous-reflection efficiencies of metagratings under three conditions. Segmentation is set on the y axis to clearly display data from different ranges. (a)–(c) Results corresponding to expected angles of (a) $\theta = 45°$, (b) 60°, and (c) 85°. The 0th, −1st, and 1st diffractive orders are depicted for three conditions including air-based metagratings in the theoretical model (gray bar), the air-based metagratings in water (yellow bar), and the underwater metagratings in water (blue bar).

exhibits a decrease. This decrease is particularly pronounced when $\theta = 85^\circ$, with the efficiency of the air-based metagratings experiencing a significant drop. A substantial portion of energy is consumed due to undesired reflections. The observed phenomenon can be attributed to the intensifying interaction between acoustic waves and structures as the reflection angle increases. As the angle becomes larger, the contribution of the fluid-structure interaction to the acoustic field becomes increasingly significant. In contrast, by the rational utilization of FSI, the underwater metagratings consistently maintain a working efficiency of 99%.

IV. EXPERIMENTAL DEMONSTRATION

The function of the underwater metagratings has been experimentally verified using the setup described in Fig. 4(a). The experimental setup included the following components and procedures. A function signal generator (AFG3022C) was utilized to generate pulsed incident plane waves at a frequency of 500 kHz, consisting of five cycles to minimize environmental interference. The pulsed incident signals were amplified using the power amplifier (RF 2100L) to ensure an adequate signal strength for the experiments. Steel underwater metagratings, fabricated using computer-numerical-control (CNC) technology, were employed to modulate the incident acoustic waves, redirecting them to the desired reflection angles of 45°, 60°, and 85°. The parameter values, a, l_1, l_2, t_1, t_2, and d, for the three metagratings were 3.999, 0.824, 0.515, 0.526, 1.155, and 0.338 mm, 3.266, 0.856, 0.436, 0.610, 1.242, and 0.277 mm, and 2.839, 0.983, 0.251, 0.263, 1.175, and 0.558 mm, respectively. The incident range of the transducer (Olympus V389-SU) was 1.5 in.; therefore, the sample height and the width have been set to 6 cm to cover the incident size of the transducer. In addition, the thickness was 2.8 mm, which aligns with the simulation presented in Fig. 2. The hydrophone (Onda HNC-1500) and oscilloscope (PXI 5124 oscilloscope) have been used for signal reception. The hydrophone measures the signal at each measurement point within a 1-μs time frame. An automated scanning platform controls the hydrophone to scan the acoustic field in 0.5-mm and 0.25-mm steps. In Figs. 4(e) and 4(f), the scanning step sizes along the x-axis and y-axis are 0.5 mm and 0.25 mm, respectively. In Fig. 4(g), the scanning step size in the x-axis direction is further refined to 0.25 mm to achieve a clear characterization of the acoustic field. The selected scanning plane is taken at the central cross section of the metagratings. Synchronized transmission and reception setups ensure the precise alignment of the transmitted acoustic waves and the received signals in time.

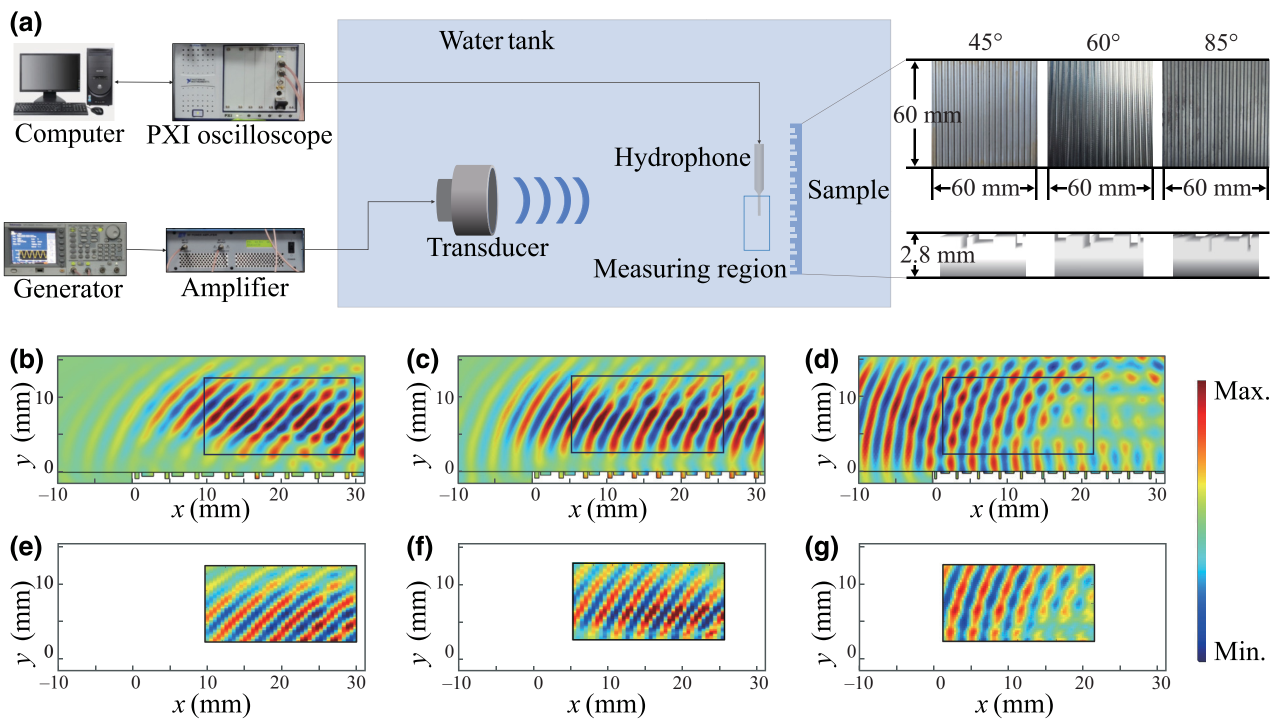

FIG. 4. The simulation and experimental results of the reflected acoustic field of the underwater acoustic metagratings. (a) The schematic diagram of the experimental system and samples, showing the lengths, widths, and thicknesses of the three samples. (b)–(d) The transient *simulation* results of plane waves incident on the three underwater metagratings with the desired reflection angle (b) $\theta = 45^\circ$, (c) 60°, and (d) 85°. (e)–(g) The *experimental* results of plane waves incident on the three underwater metagratings with the same desired reflection angles.

The forms of behavior of the three overarching designed underwater metagratings for reflection angles of 45°, 60°, and 85° are shown in Figs. 4(b)–4(g). The transient simulations are carried out to match the experimental settings and measurement methods and the measurement locations are carefully selected. The structural parameters of the metagratings are identical to those of the metal samples. The simulated acoustic fields are shown in Figs. 4(b)–4(d). Due to the disparate time frames of acoustic wave interactions within the structure, the duration needed to attain a stable reflected acoustic field varies. For the three expected reflection angles, we have selected corresponding time instances to facilitate the comparative analysis of the steady-state reflected waves between the simulation and experimental results. The width of the incident acoustic field area was 1.5 in. and the distribution size of the experimental measurement points was 2 cm × 1 cm. We have compared the experimentally measured acoustic field Figs. 4(e)–4(g) with the corresponding spatiotemporal simulated acoustic field (in the blue box). Both results are in good agreement, proving that the optimized underwater metagratings have an efficient abnormal-reflection ability.

On the other hand, there may be some differences between the simulation and experimental results.This imperfect matching can be attributed to several factors, one of which is the inability to fully guarantee the accuracy of the measurement positions. Additionally, the machining accuracy of the metagratings can also impact the efficiency, potentially contributing to the mismatch between simulation and experiment. In future work, we will further explore high frequency and adopt more precise positioning and processing methods to improve the accuracy of the experiment. The current metagrating is designed for a specific frequency, resulting in a narrow operating bandwidth of 30 kHz with 97.5% efficiency. To broaden the operating frequency range of the device, there might be a feasible way to add more subunits within a period to increase the freedom of manipulation. Furthermore, we recognize that the thickness of the back plate can play a role in optimizing the performance of the structure. By selecting an appropriate thickness, we can reduce the duty cycle of the structure and improve its overall mass density, thereby improving the reflection efficiency of the structure.

V. CONCLUSIONS

In this study, we have aimed to design underwater metagratings with efficient wave-front control. Considering the fluid-structure interaction and interaction among subunits, we have proposed an overarching optimization strategy for the design of acoustic metagratings. Compared to previous design approaches, particularly in situations involving large angles of abnormal reflection, our strategy demonstrates superior operational performance. The simulations and experimental validations have demonstrated that the designed underwater metagratings exhibit a high wave-front-modulation efficiency, with the anomalous-reflection efficiency reaching more than 99%. The design strategy proposed in this study provides a valuable reference for the development of underwater acoustic detection technologies and devices, opening new avenues to facilitate hydroacoustic manipulation. In addition, this method holds potential for enhancing acoustic stealth performance and enabling biomedical ultrasound-directed diagnosis and therapy.

ACKNOWLEDGMENTS

This work was supported in part by the National Key R&D Program of China (Grants No. 2022YFA1404400 and No. 2020YFA0211400), the National Natural Science Foundation of China (Grant No. 12034015), and the Fundamental Research Funds for the Central Universities.

[1] B. Assouar, B. Liang, Y. Wu, Y. Li, J. C. Cheng, and Y. Jing, Acoustic metasurfaces, Nat. Rev. Mater. **3**, 460 (2018).

[2] X. Wang, R. Dong, Y. Li, and Y. Jing, Non-local and non-Hermitian acoustic metasurfaces, Rep. Prog. Phys. **86**, 116501 (2023).

[3] L. Huang, S. Huang, C. Shen, S. Yves, A. S. Pilipchuk, X. Ni, S. Kim, Y. K. Chiang, D. A. Powell, J. Zhu, Y. Cheng, Y. Li, A. F. Sadreev, A. Alù, and A. E. Miroshnichenko, Acoustic resonances in non-Hermitian open systems, Nat. Rev. Phys. **6**, 11 (2024).

[4] Y. Li, B. Liang, Z. M. Gu, X. Y. Zou, and J. C. Cheng, Reflected wavefront manipulation based on ultrathin planar acoustic metasurfaces, Sci. Rep. **3**, 2546 (2013).

[5] J. Zhao, B. Li, Z. Chen, and C. W. Qiu, Manipulating acoustic wavefront by inhomogeneous impedance and steerable extraordinary reflection, Sci. Rep. **3**, 2537 (2013).

[6] Y. Xie, W. Wang, H. Chen, A. Konneker, B.-I. Popa, and S. A. Cummer, Wavefront modulation and subwavelength diffractive acoustics with an acoustic metasurface, Nat. Commun. **5**, 5553 (2014).

[7] G. Ma, M. Yang, S. Xiao, Z. Yang, and P. Sheng, Acoustic metasurface with hybrid resonances, Nat. Mater. **13**, 873 (2014).

[8] X. Jiang, Y. Li, B. Liang, J.-C. Cheng, and L. Zhang, Convert acoustic resonances to orbital angular momentum, Phys. Rev. Lett. **117**, 034301 (2016).

[9] X. Wang, D. Mao, and Y. Li, Broadband acoustic skin cloak based on spiral metasurfaces, Sci. Rep. **7**, 11604 (2017).

[10] S. Qi, Y. Li, and B. Assouar, Acoustic focusing and energy confinement based on multilateral metasurfaces, Phys. Rev. Appl. **7**, 054006 (2017).

[11] Y. Li, C. Shen, Y. Xie, J. Li, W. Wang, S. A. Cummer, and Y. Jing, Tunable asymmetric transmission via lossy acoustic metasurfaces, Phys. Rev. Lett. **119**, 035501 (2017).

[12] B.-I. Popa, Y. Zhai, and H.-S. Kwon, Broadband sound barriers with bianisotropic metasurfaces, Nat. Commun. **9**, 5299 (2018).

[13] K. Song, J.-H. Kwak, J. J. Park, S. Hur, M. Anzan-Uz-Zaman, and J. Kim, Acoustic beam forming based on a

surface with sinusoidally modulated admittance, Phys. Rev. Appl. **10**, 044025 (2018).

[14] A. Díaz-Rubio, J. Li, C. Shen, S. A. Cummer, and S. A. Tretyakov, Power flow–conformal metamirrors for engineering wave reflections, Sci. Adv. **5**, eaau7288 (2019).

[15] X. Wang, X. Fang, D. Mao, Y. Jing, and Y. Li, Extremely asymmetrical acoustic metasurface mirror at the exceptional point, Phys. Rev. Lett. **123**, 214302 (2019).

[16] R. Ghaffarivardavagh, J. Nikolajczyk, S. Anderson, and X. Zhang, Ultra-open acoustic metamaterial silencer based on Fano-like interference, Phys. Rev. B **99**, 024302 (2019).

[17] S. Huang, Z. Zhou, D. Li, T. Liu, X. Wang, J. Zhu, and Y. Li, Compact broadband acoustic sink with coherently coupled weak resonances, Sci. Bull. **65**, 373 (2020).

[18] N. Jiménez, J.-P. Groby, and V. Romero-García, Spiral sound-diffusing metasurfaces based on holographic vortices, Sci. Rep. **11**, 10217 (2021).

[19] Y. K. Chiang, L. Quan, Y. Peng, S. Sepehrirahnama, S. Oberst, A. Alù, and D. A. Powell, Scalable metagrating for efficient ultrasonic focusing, Phys. Rev. Appl. **16**, 064014 (2021).

[20] H. Xie and Z. Hou, Nonlocal metasurface for acoustic focusing, Phys. Rev. Appl. **15**, 034054 (2021).

[21] H. Esfahlani, Y. Mazor, and A. Alù, Homogenization and design of acoustic willis metasurfaces, Phys. Rev. B **103**, 054306 (2021).

[22] Y. Zhu, A. Merkel, K. Donda, S. Fan, L. Cao, and B. Assouar, Nonlocal acoustic metasurface for ultrabroadband sound absorption, Phys. Rev. B **103**, 064102 (2021).

[23] Z. Zhou, S. Huang, D. Li, J. Zhu, and Y. Li, Broadband impedance modulation via non-local acoustic metamaterials, Natl. Sci. Rev. **9**, nwab171 (2022).

[24] M. Malléjac, P. Sheng, V. Tournat, V. Romero-García, and J. P. Groby, Slow-sound-based delay-line acoustic metamaterial, Phys. Rev. Appl. **17**, 044035 (2022).

[25] M. Xu, W. S. Harley, Z. Ma, P. V. S. Lee, and D. J. Collins, Sound-speed modifying acoustic metasurfaces for acoustic holography, Adv. Mater. **35**, 2208002 (2023).

[26] Z. Zhou, B. Jia, N. Wang, X. Wang, and Y. Li, Observation of perfectly-chiral exceptional point via bound state in the continuum, Phys. Rev. Lett. **130**, 116101 (2023).

[27] N. Y. Wang, C. C. Zhou, S. Qiu, S. B. Huang, B. Jia, S. S. Liu, J. M. Cao, Z. L. Zhou, H. Ding, J. Zhu, and Y. Li, Metasilencer with designable timbre, Int. J. Extrem. Manuf. **5**, 025501 (2023).

[28] J. Mei, G. Ma, M. Yang, Z. Yang, W. Wen, and P. Sheng, Dark acoustic metamaterials as super absorbers for low-frequency sound, Nat. Commun. **3**, 756 (2012).

[29] R.-Q. Li, B. Liang, Y. Li, W.-W. Kan, X.-Y. Zou, and J.-C. Cheng, Broadband asymmetric acoustic transmission in a gradient-index structure, Appl. Phys. Lett. **101**, 263502 (2012).

[30] Y. Li, B. Liang, X. Tao, X.-F. Zhu, X.-Y. Zou, and J.-C. Cheng, Acoustic focusing by coiling up space, Appl. Phys. Lett. **101**, 233508 (2012).

[31] N. Yu, P. Genevet, M. A. Kats, F. Aieta, J.-P. Tetienne, F. Capasso, and Z. Gaburro, Light propagation with phase discontinuities: Generalized laws of reflection and refraction, Science **334**, 333 (2011).

[32] A. Díaz-Rubio and S. A. Tretyakov, Acoustic metasurfaces for scattering-free anomalous reflection and refraction, Phys. Rev. B **96**, 125409 (2017).

[33] Y. Jin, X. Fang, Y. Li, and D. Torrent, Engineered diffraction gratings for acoustic cloaking, Phys. Rev. Appl. **11**, 011004 (2019).

[34] H. Ni, X. Fang, Z. Hou, Y. Li, and B. Assouar, High-efficiency anomalous splitter by acoustic meta-grating, Phys. Rev. B **100**, 104104 (2019).

[35] Z. Hou, X. Fang, Y. Li, and B. Assouar, Highly efficient acoustic metagrating with strongly coupled surface grooves, Phys. Rev. Appl. **12**, 034021 (2019).

[36] Z. Hou, H. Ding, N. Wang, X. Fang, and Y. Li, Acoustic vortices via nonlocal metagratings, Phys. Rev. Appl. **16**, 014002 (2021).

[37] H. Ding, X. Fang, B. Jia, N. Wang, Q. Cheng, and Y. Li, Deep learning enables accurate sound redistribution via nonlocal metasurfaces, Phys. Rev. Appl. **16**, 064035 (2021).

[38] J. He, X. Jiang, D. Ta, and W. Wang, Experimental demonstration of underwater ultrasound cloaking based on metagrating, Appl. Phys. Lett. **117**, 091901 (2020).

[39] H.-T. Zhou, W.-X. Fu, Y.-F. Wang, and Y.-S. Wang, High-efficiency ultrathin nonlocal waterborne acoustic metasurface, Phys. Rev. Appl. **15**, 044046 (2021).

[40] L. Fan and J. Mei, Metagratings for waterborne sound: Various functionalities enabled by an efficient inverse-design approach, Phys. Rev. Appl. **14**, 044003 (2020).

[41] COMSOL, Acoustic-structure interaction.